



Climatology of low-level temperature inversions over China based on high-resolution radiosonde measurements

Qianqian Huang¹ · Yiqi Chu² · Qianhui Li³

Received: 17 July 2020 / Accepted: 13 January 2021 / Published online: 11 February 2021
© The Author(s), under exclusive licence to Springer-Verlag GmbH, AT part of Springer Nature 2021

Abstract

Low-level temperature inversions play crucial roles in inhibiting vertical exchange of energy and mass, and may lead to air pollutants accumulation. The climatological study of them provides a fundamental overview of the static stability of atmosphere and is indispensable for air pollution controls. Based on high-vertical-resolution radiosondes at 00 and 12 UTC during 2011–2018, this work comprehensively examined the spatial and temporal variability of three characteristics (occurrences, strengths, and depths) of low-level inversions in China. Results revealed that inversions are prevalent (more than 80% of the observation records) over Eastern China. The northern part of Eastern China is dominated by the thick strong surface-based inversions with median thickness and strength of 200 m and 3 K, while the southern part by thin weak elevated ones of 80 m and 0.8 K. Tibetan Plateau experiences rare inversions (less than 50% of the time) which tend to be strong thick surface-based inversions with median depth and intensity of 170 m and 4 K. Inversion depths and strengths are positively correlated. The three properties of inversions present remarkable seasonal variations. Generally, inversions are strongest, thickest, and most frequent in winter and least so in summer, with median intensity and depth ranging from 0.3 K and 80 m to 5 K and 220 m. This paper also analyzed the monthly variations of inversions of four representative stations (Harbin, Urumqi, Beijing, and Chongqing) in details. These four cities are known for frequent severe air pollution events. The quantitative investigations of inversions may play a significant role in atmospheric environmental management.

Keywords Low-level temperature inversions · Surface-based inversions · Elevated inversions · Climatology · China

1 Introduction

A temperature inversion refers to a layer of atmosphere where the temperature increases with altitude. In respect to their base heights, two types of temperature inversions have been distinguished: surface-based temperature inversions (SBIs) starting from the ground and elevated inversions (EIs) whose bottoms locate above the ground. The formation mechanisms of inversions have been substantially explored. SBIs usually form

after sunset because of the radiative cooling of the ground, and gradually grow in depth and strength. They usually dissipate after sunrise or are destroyed by winds stronger than 20 km/h (Czarnecka et al. 2019). Leukauf et al. (2015) claimed that for an idealized valley, a minimum energy about 450 W/m^2 is required to destroy a persistent inversion. Warm air advections above a cooler surface could also result in the development of SBIs. EIs are usually generated by warm advections, or subsidence of air parcels associated with high-pressure systems, fronts, or plateau-plain topography and valleys (Largerion and Staquet 2016; Vihma et al. 2011; Palarz et al. 2019; Zhu et al. 2018). They may also appear as remnants of SBIs during the morning when SBIs are destroyed by surface heating (Palarz et al. 2019; Stryhal et al. 2017). Low-level inversions may also be influenced by clouds, turbulence, and so on (Tjernstrom and Graversen 2009; Zhang et al. 2011a).

Considerable literature has focused on inversions of polar regions, trying to improve the understanding of polar amplification, the photochemical destruction of boundary layer ozone

✉ Yiqi Chu
chuyiqi@pku.edu.cn

¹ Institute of Urban Meteorology, China Meteorological Administration, Beijing, People's Republic of China

² Beijing Institute of Radio Measurement, Beijing, People's Republic of China

³ Laboratory for Climate and Ocean-Atmosphere Studies, Department of Atmospheric and Oceanic Sciences, School of Physics, Peking University, Beijing 100871, People's Republic of China

at sunrise, the modeling of sea ice movement, and climate feedback mechanisms (Kahl et al. 1996; Pietroni et al. 2014; Tjernstrom and Graversen 2009; Zhang et al. 2011a; Zhang et al. 2011b). For China, we are more concerned about their environmental influences. Temperature inversions significantly suppress mass and energy exchanges, and therefore result in weak winds and high moisture environment, and restrict the dispersion of air pollutants (Nidzgorska-Lencewicz and Czarnecka 2015). Trapped moisture in favor of chemical reactions of secondary aerosols further aggregates air pollutions (Zhong et al. 2017; Wu et al. 2018). Numerous studies have proved through case study and statistical research that haze events are mainly attributed to unfavorable weather conditions, especially the static stable atmosphere; in that, the emissions of air pollutants usually remain unchanged for a particular region during a short period (Huang et al. 2018). For example, Shi et al. (2020) reported a pollution case when deep strong elevated inversion caused a rapid increase of PM_{2.5} in central east China. Zhong et al. (2019) investigated winter haze events during 2014–2016, and concluded that weak winds, strong inversions, and shallow boundary layers are conducive to severe haze. According to Xu et al. (2019), there is a robust linear relationship between inversion strength and PM_{2.5} concentrations in North China, where temperature inversions occur in 93% of severe polluted days. Gramsch et al. (2014) claimed that on days with inversions, PM_{2.5} was 84% higher than the days without. Therefore, a better understanding of the behavior of temperature inversions is indispensable for air pollution control.

Plenty of climatological studies have been made about low-level temperature inversions of polar regions. For instance, Jakobson et al. (2013) studied climatological features of low-level temperature inversions and their correlations with the low-level jets in the stably stratified atmospheric boundary layer. Wetzel and Brummer (2011) investigated the occurrence frequency, depth, and strength of boundary-layer inversions in the Arctic based on ERA-40 reanalysis data during 1957–2002. Zhang et al. (2011a) examined the spatial and temporal variability of surface-based inversions based on radiosonde observations of both polar regions, and checked the validity of two climate models and one reanalysis dataset. In contrast, climatological properties of low-level inversions have not been fully characterized in mid-latitude regions. Based on radiosonde observations, inversion activities were quantified for the Southern Great Plains in north Oklahoma (Li et al. 2015a), Alaska (Bourne et al. 2010), one valley of the western USA (Wang et al. 2015), southwest USA (Bailey et al. 2011), the USA (Zhang et al. 2011b), eastern England (Milionis and Davies, 2008), Indochina Peninsula (Nodzu et al. 2006), northern coastal Chile (Munoz et al. 2011), Athens (Prezerakos 1997; Katsoulis 1988), and Oman (Abdul-Wahab et al. 2004, 2005). Inversion features were also examined based on weather masts observations by Brummer

and Schultze (2015) for Hamburg, reanalysis data by Palarz et al. (2019) for Europe, and climate models by Ji et al. (2018) for Australia. There were few fragmentary studies for some particular cities in China. For example, Xia et al. (2017) examined the characteristics of elevated and surface-based inversions during 2010–2015 in Nanjing city; Guo et al. (2014) investigated the variation of inversions during 2006–2012 and discussed their relationships with air quality. Therefore, a comprehensive investigation of the climatological characteristics of inversions in China is necessary.

China has great physical diversity. The average altitude of Tibetan Plateau in the southwest is over 4000 m, but is less than 50 m for the eastern plain area. Between Tibetan Plateau and the eastern plain area, there are plateaus like Inner Mongolian Plateau and Loess Plateau, and basins like Sichuan Basin and Tarim Basin. The climate of China is also tremendously diverse, ranging from tropical in the southernmost province (Hainan) to subarctic in the northernmost (Heilongjiang). The great physical and climate diversity results in distinctive meteorological phenomena, making it a challenge to analyze the features of low-level inversions in China.

Temperature profiles from radiosonde observations are most commonly used dataset, since sounding profiles are usually more accurate and have higher vertical resolutions compared to reanalysis data and climate model results (Liu et al. 2006; Tjernstrom and Graversen 2009; Zhang et al. 2011a). However, radiosondes with standard and significant pressure levels may still not be able to detect strong shallow inversion layers or may sample elevated inversions as surface-based ones (Kahl et al. 1996; Mahesh et al. 1997; Seidel et al. 2010; Zhang et al. 2011a; Pietroni et al. 2014). This is especially significant for studies of air pollution, since shallow layers may have a strong restraining effect on pollutants and result in serious pollution events. As a consequence, the strong and shallow inversions along with severe air pollution may be underestimated. In this study, we use high-resolution (about 8 m) radiosondes to more precisely quantify the structure of inversions.

The main goal of our research is to present an overview of the characteristics of low-level temperature inversions in China, based on high-vertical-resolution radiosonde observations during 2011–2018. The spatial and temporal variability of occurrence frequency, thickness, and strength of both surface-based and elevated inversions are investigated.

2 Data and methods

The radiosonde data used in this study are from L-band sounding system maintained by the China Meteorological Administration (CMA). The CMA began to update its radiosonde system in 2002, and finished the building of the L-band

sounding system in 2011. This system consists of 120 stations across China, and provides high-resolution profiles of pressure, height, temperature, relative humidity, wind speed, and wind direction twice a day at 0000 and 1200 UTC (i.e., 0800 and 2000 China Standard Time). The vertical resolution of the L-band radiosonde data is approximately 8 m. Compared to the sounding profiles with only standard and significant pressure levels, L-band radiosonde data are able to more precisely describe the details of the structure of the atmosphere, especially the low-level inversions. Taking temperature profile at 2013010300 UTC from Harbin station as an example (Fig. 1), the significant sounding level for temperature below 1000 m (above the ground level, a.g.l.) was not determined correctly. As a result, the thickness of SBI identified from coarse vertical resolution profile is about 664 m. However, based on fine-resolution profile, the thickness is much shallower (only 288.7 m).

We obtained long-term (2011–2018) fine-resolution radiosondes of 120 stations across China to investigate the characteristics of temperature inversions. All soundings were checked for their quality and completeness. First, soundings were manually inspected to ensure that no obviously erroneous values occur in the data of temperature and height. Obviously high or low temperatures were removed. Second, the surface temperature was regarded as missing if there was no temperature record within 10 m a.g.l. and the corresponding profiles were removed from the analysis. After the quality control, more than 95% of the data for 119 stations are valid, except for station 58927, where 63.7% of the data were missing. Therefore, we use data from 119 stations in this research. Figure 2 displays the distribution of stations. It is shown that 119 stations cover all of contiguous China well, although there are relatively fewer stations over the western Tibet. This dataset is considered sufficient to conduct climatological research on temperature inversions over China.

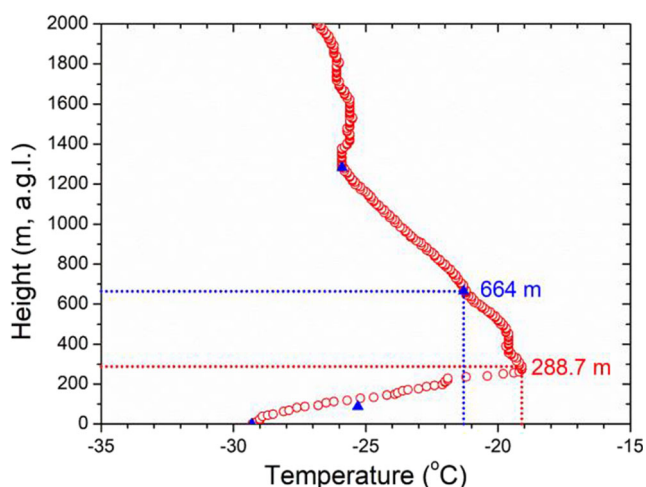


Fig. 1 Comparisons between L-band radiosondes with high vertical resolutions (red) and original radiosondes (blue) with only standard and significant pressure levels at 2013010300 UTC of Harbin station (50953)

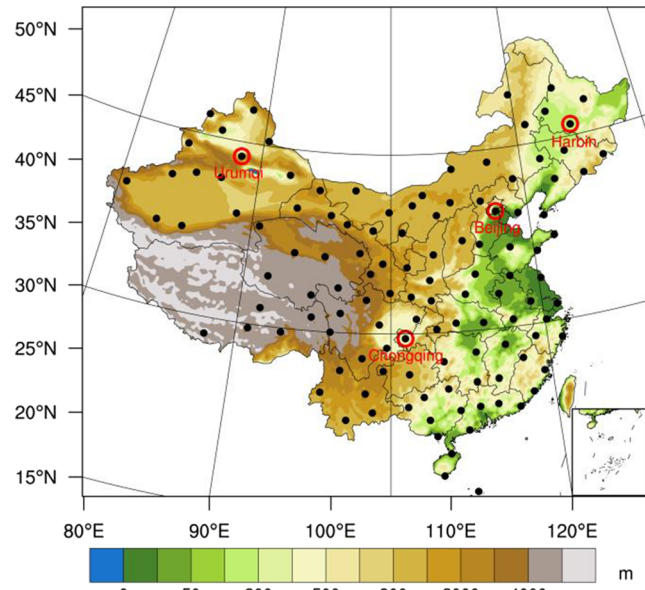


Fig. 2 Distributions of radiosonde stations. The red circles indicate the four representative stations (Harbin, Urumqi, Beijing and Chongqing)

Following the detection algorithm of Kahl (1990), low-level inversions over China were objectively identified. Each temperature profile was scanned upward from the surface. The bottom of the first layer where the temperature increases with altitude was defined as the inversion base, and the bottom of the first subsequent layer where the temperature decreases with the altitude was defined as the inversion top. An individual temperature profile often has a complicated structure. In many cases, multiple inversion layers occur in one profile. Two neighboring inversion layers separated by a thin embedded non-inversion layer (< 100 m) were merged to be one deeper inversion layer. We examined the sensitivity of the climatological statistics of inversions to this thickness threshold by testing thickness values of 10, 50, 100, 150, and 200 m. It showed that when thicker non-inversion layers are tolerated, we obtained thicker and stronger inversions as expected. For example, inversions with 150-m threshold are 20 m thicker and 0.1 K stronger than those with 100-m threshold. Given that the precedent literature adopted 100-m threshold (e.g., Kahl 1990; Liu et al. 2006), our analyses also follow this standard for better comparisons.

Dataset of inversions are passed through a series of limits check. First, any inversion layer that is shallower than 20 m (Tjernstrom and Graversen 2009) or whose top is higher than 3000 m was removed from this analysis. Since we are mainly concerned about the vertical mixing extent of pollutants in the lower atmosphere, 3000 m a.g.l. is chosen as the reasonable upper limit for the investigation of low-level inversions in China,. An inversion was determined as a surface-based inversion if its base height is lower than 10 m a.g.l.; otherwise, it was regarded as an elevated inversion. Only the lowermost inversion layer was taken into consideration in this research,

because it exerts dominant influence on vertical exchange of near-surface air pollutions. This treatment is consistent with the previous studies carried out by Czarnecka et al. (2019), Palarz et al. (2019), etc.

Three parameters are used to describe the characteristics of inversions in our research: inversion depth (ΔH), inversion strength (ΔT), and inversion frequency. For elevated inversions, the characteristics of their base height are also investigated. The inversion depth is the height difference between the top and bottom of the inversion layer, and the inversion strength is defined as the corresponding temperature difference between these two levels. Following the equations described by Kahl et al. (1996), the inversion frequency for SBI and EI are defined as F_{SBI} and F_{EI} , respectively:

$$F_{SBI} = N_{SBI}/(N_{SBI} + N_{EI}),$$

$$F_{EI} = N_{EI}/(N_{SBI} + N_{EI}),$$

where N_{SBI} and N_{EI} are the number of SBI and EI, respectively. F_{SBI} and F_{EI} quantify the proportion of SBI and EI in all inversions, respectively. Median features of these three parameters are investigated, including the climatological characteristics of spatial distribution, seasonal and monthly variations. Median values are chosen instead of mean values, because medians are less prone to outliers. In order to show the spatial distribution of inversion frequency, thickness, and strength over continental China, the results of 119 stations have been spatially interpolated by tension splines.

3 Results and discussions

3.1 Inversion occurrence

The occurrences of low-level temperature inversions are distributed with substantial regional heterogeneity (Fig. 3a). They appear most frequently over eastern plains where the occurrence frequency is more than 80% and decrease in frequency westward. Over Tibetan Plateau, the inversions only occur 40% of the time, due to the unique thermal and dynamical factors there. High altitude of Tibetan plateau corresponds to stronger solar radiation, thinner air, and less moisture (Chen et al. 2014; Zhu et al. 2010) which enhance thermal convections, create strong turbulent mixings, and make inversions harder to form and easy to be dissolved. Moreover, the strong winds brought by westerly jet stream (Schiemann et al. 2009) also contribute to disturb the formation of inversions and expedite their collapse. The distribution pattern of low-level inversion occurrences agrees well with that of atmospheric boundary layer height reported by Huang et.al (2018) and Guo et al. (2016). It suggests that low-level inversions actually represent the characteristics of the boundary layer (Pietroni et al. 2014).

The occurrence frequency of SBI, i.e., the proportion of surface-based inversions among all inversions, shows a different distribution pattern (Fig. 3b). SBIs are most prevalent over the western regions where they account for more than 70% of all inversions, and rarely occur over the southeast region. It suggests that inversions in the west are more likely to become a surface-based type rather than an elevated one. This distribution well follows the pattern of diurnal temperature range (DTR) demonstrated in the study by Liu et al. (2016). Larger DTR in the west indicates enough cooling of the surface which allows SBI to form and persist for longer time. Another reason is that the twice daily sounding profiles provide instantaneous snapshots of atmospheric thermal structures which are highly related to their local sampling times. Geographically, China covers five time zones. However, sounding profiles are sampled twice a day at two universal times: 0000 and 1200 UTC. For eastern China, 0000 and 1200 UTC are about 0800 and 2000 true solar time, representing the early-morning and early-evening conditions, respectively. Sounding profiles of the east may capture the thermal structures when SBIs have already been dissolved or just before their formation, leading to fewer SBIs in the east in Fig. 3b. For western China, 0000 and 1200 UTC are equivalent to about 0500 and 1700 true solar time, respectively, representing the before-dawn conditions when SBIs have been prosperously developed and afternoon conditions when inversions rarely occur. Therefore, western China exhibits large proportion of SBIs. When it comes to studies related to atmospheric boundary layers, it would be beneficial if radiosondes were performed at the time of local maximum and minimum daily temperatures (Seidel et al. 2012) instead of a universal time (Greenwich Meridian Time). Since F_{EI} is the complement of F_{SBI} , the spatial distribution pattern of F_{EI} is opposite to that of F_{SBI} (Figure not shown). We only elaborate the distribution of F_{SBI} here.

In summary, inversions occur prevalently over the east of China. They tend to be SBIs over the northern part of eastern China, and EIs over the southern part. Inversions over the west of China occur less frequently, especially those over Tibetan Plateau, and they are inclined to be SBIs.

Inversion frequencies display a pronounced seasonal variation (Fig. 4). Generally, inversions are most popular in cold seasons and relatively rare in warm ones. In summer, only the east and southeast plains experience frequent inversions with a frequency of more than 70%. The chance for the rest areas to experience inversions is less than 50%. Areas with prevalent inversions gradually spread westward from summer to winter. All areas exhibit a wintertime inversion frequency in excess of 70%, except for Tibetan Plateau where inversions occur less than half the time.

The occurrence of SBI was also found to be more popular in winter than that in summer. During warm seasons, only the northwest part of China is most likely to exhibit SBIs where

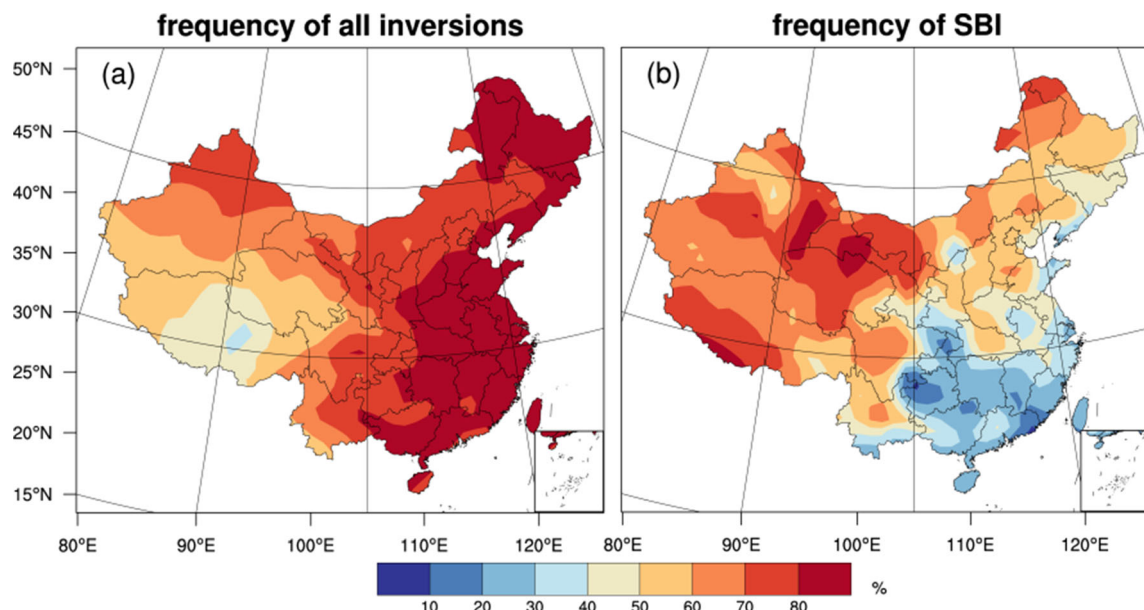


Fig. 3 Spatial distribution of the occurrence frequency of all inversions (a) and SBI (b) during 2011–2018

they account for more than 70% of all inversions, while in other regions, the proportion ranges from 10 to 50%. During cold seasons, the majority of the country experiences a large SBI proportion, except for a small region in the southeast. This is reasonable because longer nights in winter result in sufficient cooling of the ground which contributes to the development of SBIs. Meanwhile, there are more occasions during winter morning when SBIs cannot be broken through due to weak surface heating at the time the sounding observations were made. This is in line with the analyses of Seidel et al. (2010) and Abdul-Wahab (2003), etc.

To conclude, all regions experience more SBIs in winter than those in summer. The west of China is dominated by SBIs all season, whereas the southeast by EIs all year around. The northeast of the country tends to exhibit SBIs in winter and EIs in summer.

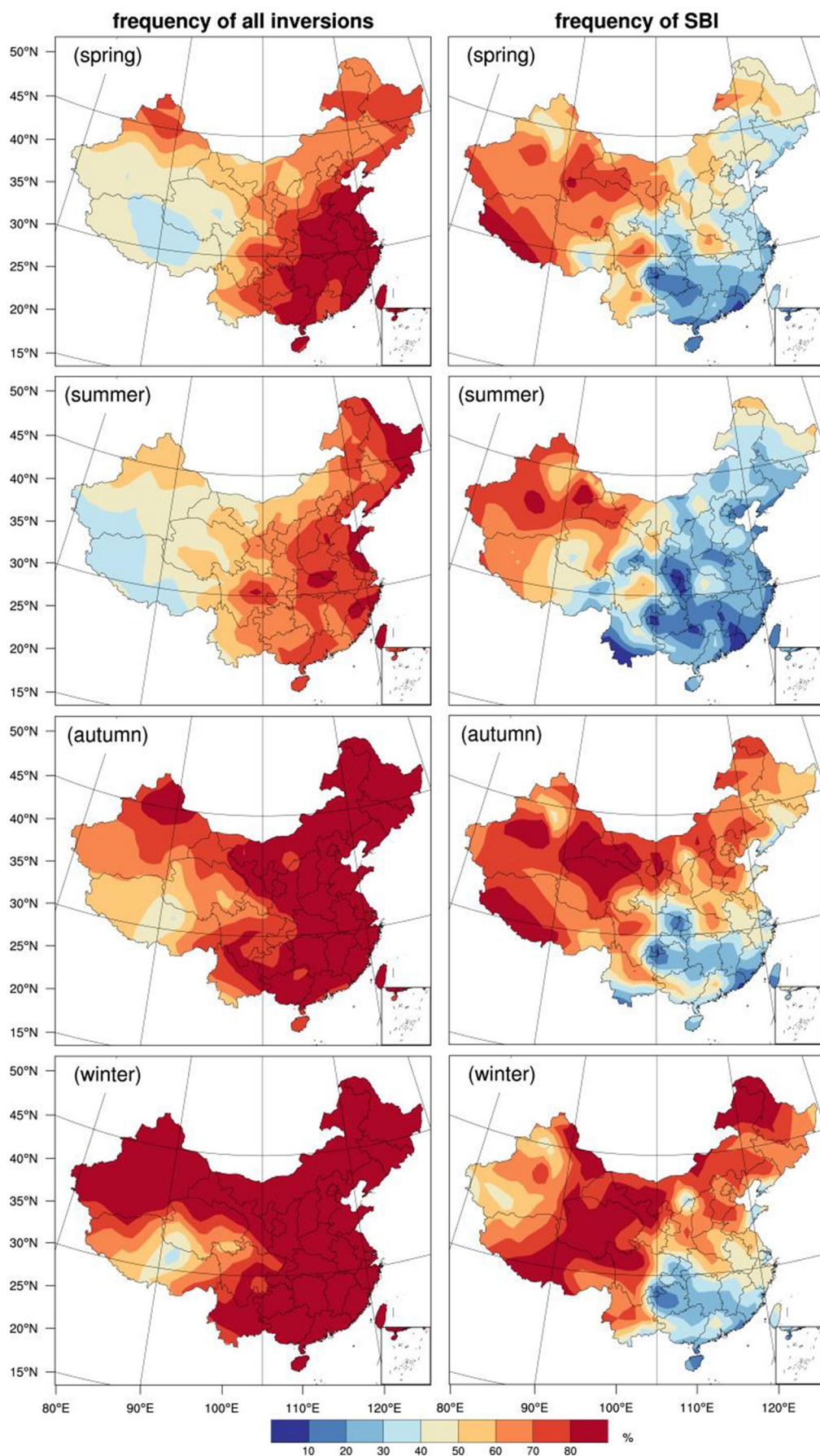
Four representative stations are selected (Harbin, Urumqi, Beijing, and Chongqing, shown in Fig. 2) to examine the detailed monthly variation of inversion frequency (Fig. 5). Harbin, Urumqi, Beijing, and Chongqing are known for frequent severe air pollutions (e.g., Cai et al., 2017; Li et al., 2015b; Liao et al., 2018; Xu et al., 2017). It is necessary to discuss their characteristics of inversions in details. Choosing these four stations is also a continuation of our previous research (Huang et al., 2017; Huang et al., 2018), in which air stagnation index of China was examined. As two typical cities in northern China, Harbin, and Beijing exhibit evident monthly variations of inversion occurrences. They occur most frequently in January (98.1 and 90.5%), and least in April (65.6%) and June (63.2%). Known as “the City of Ice” in China for its long cold snowy winters and short cool summers, Harbin displays a higher frequency of inversion occurrences.

The monthly variations of surface-based and elevated inversions are also remarkable. Surface-based inversions of both stations are dominant during cold months, while elevated ones during warm months. Inversion frequency of Urumqi also exhibits a notable monthly variation. It reaches its maximum in January (95.4%) and drops to a minimum (47.3%) in June. SBIs and EIs, however, show no pronounced seasonal variations. Occurrences of both types remain nearly constant during the year, with an average frequency of about 50%. The monthly variations of inversion frequencies including both types are less obvious at Chongqing site. Inversion frequency of all types remains almost constant (about 75%) during the year. Elevated inversions appear more frequently all year around with F_{EI} ranging from 52.9% in April and August to 72% in June. Cold air masses streaming down from mountains around force warm air parcels in Sichuan Basin to be lifted, and may therefore be responsible for the frequent EIs in Chongqing.

3.2 Inversion thickness

Inversion thickness is the height difference between the base and top of the inversion layer. Thick inversions trap more air pollutants and moisture, and require more energy to be dissolved (e.g., Kassomenos et al. 2014; Thomas et al. 2019).

Generally, the thick inversions are observed over the north and west regions with a depth ranging from 140 to 200 m, whereas the south and east part exhibit thin inversions with a depth of less than 100 m (Fig. 6). A similar pattern is also found in the spatial distribution of SBI, except that the inversion depth of SBI over the north and west region is deeper (more than 180 m). Compared to SBI, the depth of EI is much



◀ Fig. 4 Seasonal variation of the occurrence frequency of all inversions (left column) and SBI (right column) during 2011–2018

thinner. The thickest EI was reported in the northeast part of China with a depth of about 120 m, whereas the thinnest was observed over Tibetan Plateau with a thickness of less than 60 m.

Combined with the characteristics of inversion occurrences in Section 3.1, we can see that the southeast of China experiences inversions frequently, and they usually are thin EIs, whereas the frequent inversions over the northeast region may have a larger chance to be thick SBIs and sometimes thick EIs also. There are fewer chances for inversions to occur over the west of China. Once an inversion has developed, it probably is a thick surface-based one.

The inversion depth also exhibits a pronounced seasonal variation (Fig. 7). Generally, inversions as well as both surface-based and elevated types are thinnest in summer and thickest in winter. Since the depth of SBIs is usually much thicker than that of EIs, the statistical results of all inversion depths well follow those of SBIs. During summer, the median depth of SBIs over majority of China is less than 80 m, except for some small discrete areas like Taklimakan Desert, Junggar Basin, and Ala Shan Desert, where the median depth is about 180 m. During winter, SBIs over plateaus like Inner Mongolia Plateau, Yunnan-Kweichow Plateau, and Tibetan Plateau and arid areas like Junggar Basin are the thickest with a median

depth of about 220 m. Plateaus usually experience frigid winter nights that favor the formation of deep SBIs. Arid and semi-arid areas receive little precipitation during winter dry seasons. Low soil moisture facilitates heat loss after sunset, leads to a rapid cooling down of the surface, and makes it easy to develop deep SBIs. Northeast China Plain also exhibits thick SBIs owing to the freezing winter of high latitudes. The depth of EI also shows a strong seasonal variation. It is generally thicker during cold months (EIs > 120 m are much more frequent) and shallower during warm months (EIs < 100 m predominated). The thickest EIs are mainly observed in winter over the southeast and northeast regions, as well as Junggar Basin in the northwest, with a median depth of 217 m.

Monthly variation of inversion depth as well as the inversion base and top at four representative stations is shown in Fig. 8. It is seen that each station displays a unique variation of inversion depth. For Harbin, the base and top of all inversions are higher in warm months and lower in cold months. Actually, the median base of all inversions is located above the ground during warm months and at the ground during cold months. It demonstrates that EI is dominant in warm months while SBI in cold months, which is in accordance with the occurrence frequencies of both types shown in Fig. 5. It also shows that the inversion thickness of all inversions as well as those two types are shallower (about 100 m) during warm month and thicker (about 250 m) during cold months, indicating that inversions in cold months require more energy to be dissolved. The inversion thickness variation in Urumqi shares

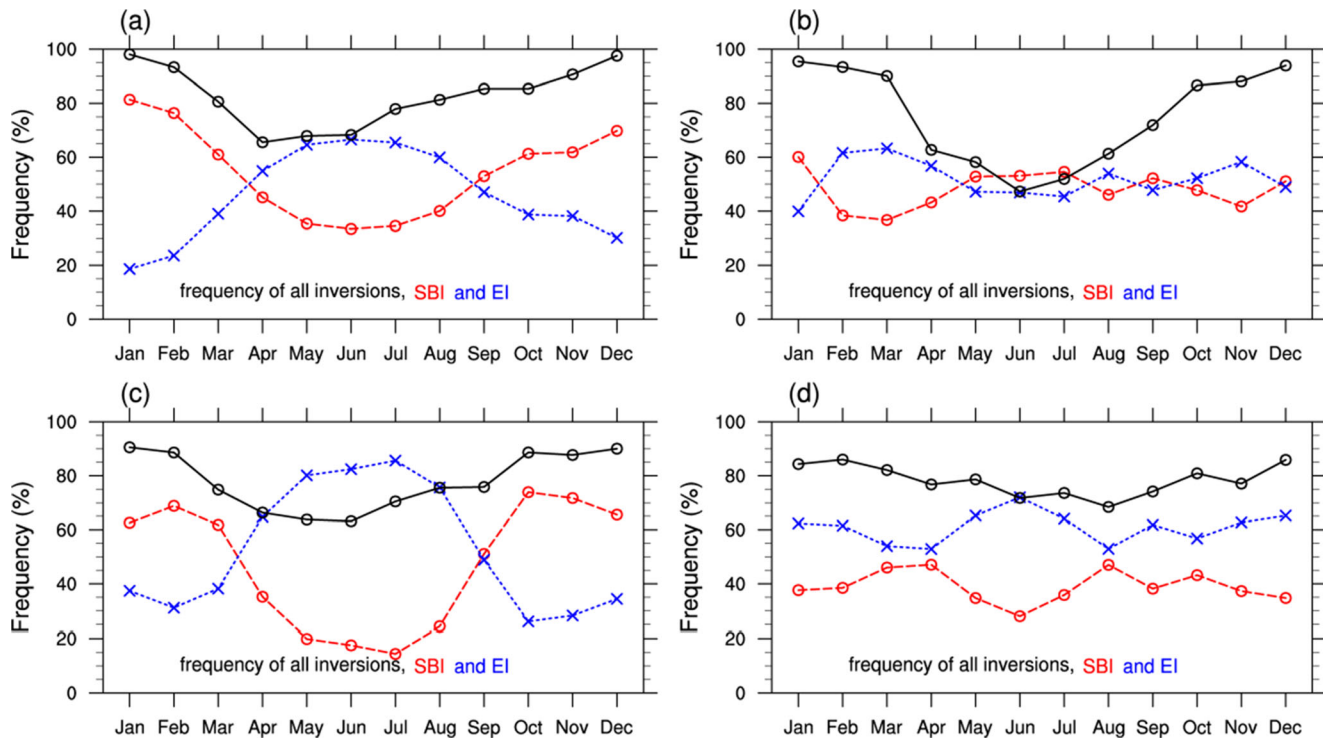


Fig. 5 Monthly variation of inversion frequency of four representative stations. **a**, **b**, **c**, and **d** stand for Harbin, Urumqi, Beijing, and Chongqing, respectively

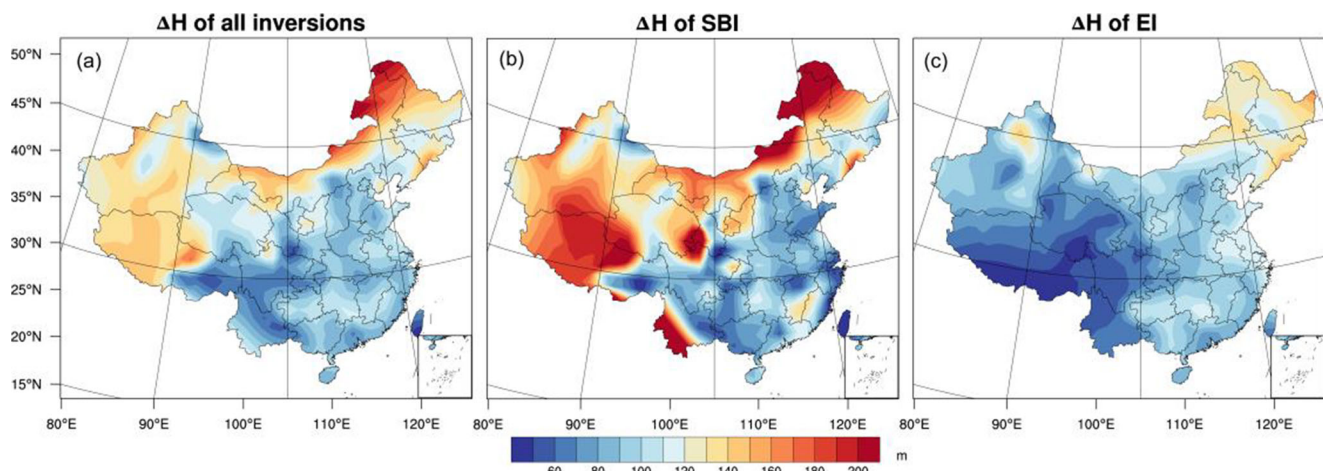


Fig. 6 Spatial distribution of median inversion thickness during 2011–2018

a similar pattern with that of Harbin, except that its inversion layers are much thicker with a median value of 200 m in summer and 500 m in winter. SBI of Urumqi varies similarly to that of Harbin but with thicker layers, due to the pooling of cold air masses in Junggar Basin (Du et al. 2018). The base height of EI in Urumqi is quite large during warm months, with a median value of about 1200 m. This may be attributed to the intense heating during the time radiosonde data were sampled. During warm months in Urumqi, the sun rises and sets at about 0630 and 2200 BJT, respectively. As a consequence, the radiosonde profiles that sampled at 0800 and 2000 BJT (i.e., 0000 and 1200 UTC) normally represent convective boundary layers during the day, and thus demonstrate higher base height of EI. The monthly variation pattern of all inversions and the SBI type in Beijing is similar to that of Harbin, except that the depth of SBI is half shallower. However, EI varies differently, the base of which locates much higher during winter than that in summer. Compared to the other three stations, inversions of both types in Chongqing are the shallowest. The median depth of SBI and EI keeps a low value (< 100 m) all year around. This may be attributed to the small DTR here (Shi, 2016). The average DTR of Chongqing reaches its maximum of 9 K in August, and drops to a minimum value of 4 K in January (Zhou 2010), which is much lower than the average DTR (ranging from 11 to 16 K) in the north and west of China (Shi 2016). The base of EI reaches its highest in February and drops to the lowest in July. Sichuan Basin locates just at the east of Tibetan Plateau which has an average elevation of 4000 m. The distinct geographical environment leads to its own unique characteristics of weather and climate. The development and maintenance of inversions are results of complex interactions between radiative forcing, synoptic activity, and so on. Further research is needed about how the nocturnal cooling of Tibetan Plateau combined with the westerly jet steam affects the behavior of inversions in Sichuan Basin.

3.3 Inversion strength

Inversion strength is defined as the temperature difference across the inversion layer. Strong inversion means more restrictions on the vertical movement of pollutants and requires more energy to be dissipated (e.g., Holmes et al. 2015; Devasthale et al. 2010).

It is shown that inversion strength exhibits a similar spatial distribution to that of inversion thickness (Fig. 9), with median temperature difference ranging from 0.5 to 4 K. Xinjiang province and the northernmost part of Heilongjiang and Inner Mongolia experience strongest and thickest inversions, whereas the southeast of China exhibits weakest and thinnest ones. Figure 9 b verifies that inversion strength shows a positive and robust correlation with thickness for all stations, so regions with thick inversions probably also experience strong ones simultaneously. Similar spatial distribution pattern was also found in SBI, except that its median intensity ranging from 0.8 to 5 K, stronger than the median value of all inversions. By contrast, elevated inversions are weak over all stations, with a median strength ranging from 0.2 to 2 K. It suggests that the strong and deep SBI may contribute dominantly in trapping air pollutants.

All inversions exhibit the same seasonal trends as do the inversion depth (Fig. 10), with a median temperature difference of less than 1 K in summer and more than 2 K in winter over the majority of China. The surface-based type varies similarly, only with a stronger intensity. Compared to the surface-based ones, the strength of elevated inversions shares the same seasonal change pattern but is weak during the whole year. The median inversion strengths of 65% stations are less than 0.5 K. Only two stations in the northeast of the country exhibit a relatively stronger strength of 1 K during summer. During winter, almost all stations experience stronger EI with a median temperature difference of more than 0.5 K. The strongest EIs located over Hulun Buir Plateau in the northeast

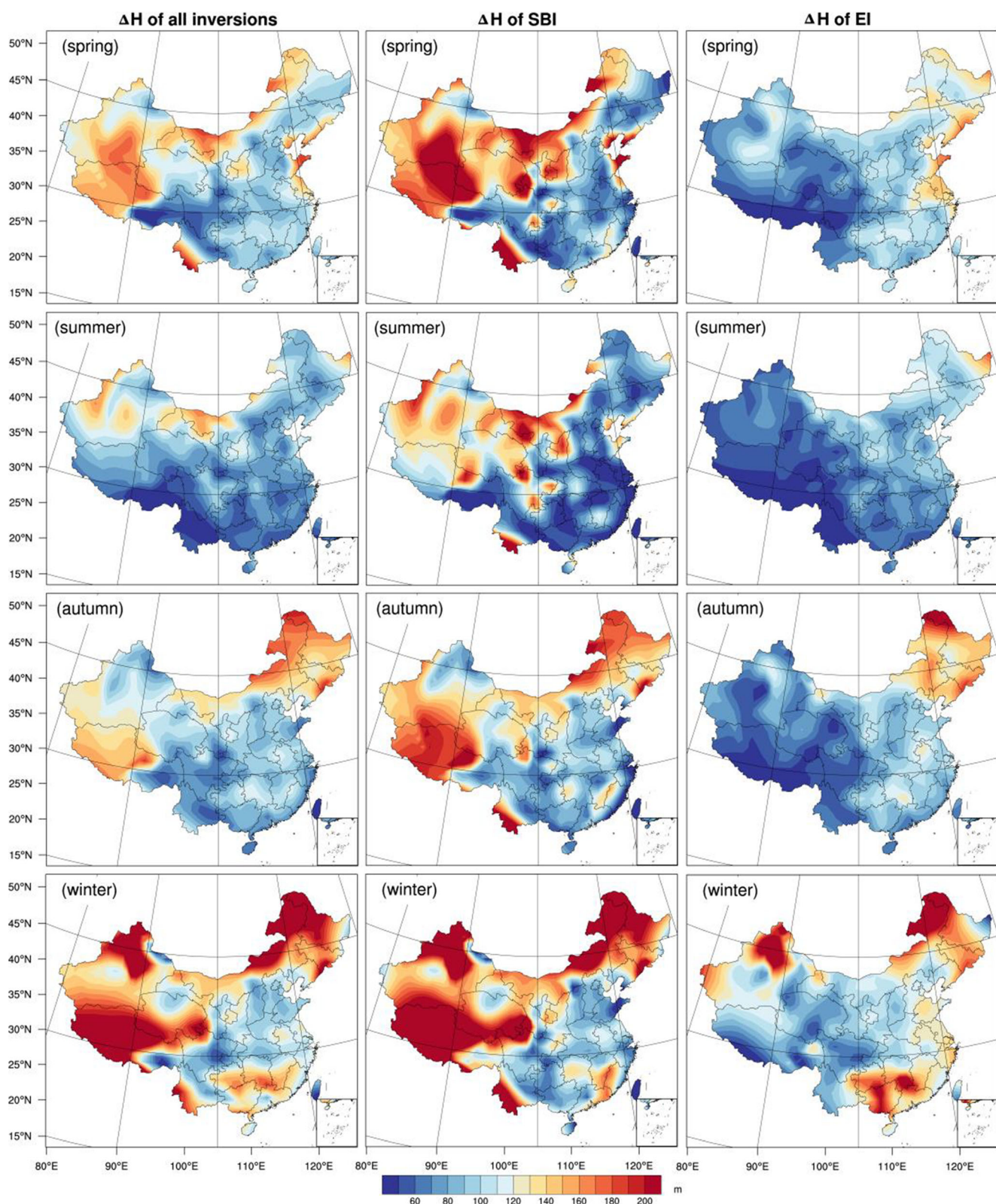


Fig. 7 Seasonal variation of the median inversion depth during 2011–2018

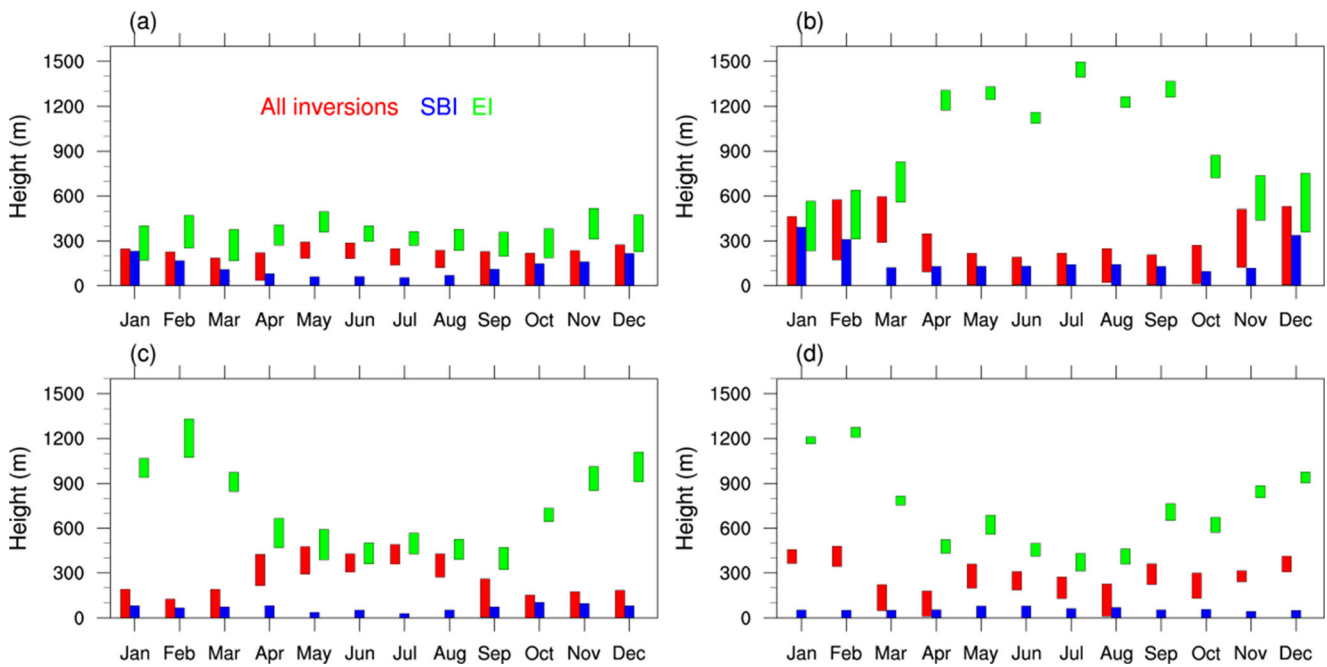


Fig. 8 Monthly variation of median inversion base (base of bars) and top (top of bars) of four representative stations. **a, b, c, and d** stand for Harbin, Urumqi, Beijing, and Chongqing, respectively

and Junggar Basin in the northwest of China, with a median strength of more than 3 K.

Specifically, for four representative stations, the monthly variation of inversion strength is quite different (Fig. 11). The intensity of inversions varies prominently in Urumqi, less pronounced in Harbin and Beijing, but keeps an almost constant low value in Chongqing. For Urumqi, inversions are strongest in January and weakest in July, with a median temperature difference ranging from 0.9 to 5.3 K. Meanwhile, the temperature differences across inversions show a large variance between 0.3 and 12.8 K in January and a relatively small one between 0.1 and 2 K in July. Elevated inversions are weaker than the surface-based ones most of the time. The inversion strength of Harbin is second to that of Urumqi, with a maximum median ΔT of 3.5 K in January and minimum value of 1 K in July. Strength of elevated inversions is nearly equal to that of surface-based ones in summer and much weaker than that in winter, which makes it less variable during the year, ranging from 0.8 to 2 K. For Beijing, all inversions, especially the surface-based type, reach their strongest in November, which explains that air pollution events are most likely to occur in late autumn. Elevated inversions, by contrast, are weak during the whole year, although the variance of ΔT is relatively large in winter, ranging from 0.2 to 4 K. Among these four stations, inversions in Chongqing are the weakest and show almost no variation during the whole year. The median temperature difference keeps to be about 0.5 K with little variance ranging from 0.1 to 2 K. It seems that inversions in Chongqing are thinnest and weakest, and thus ought to be

less favorable to pollutants accumulations. However, according to Feng et al. (2020), multiple inversion layers often occur below 3000 m in Sichuan Basin, which seriously deteriorate the ventilation conditions. The adjacent Tibetan Plateau and the mountain-basin topography combined with complex weather circumstances complicate the characteristics of inversions in Sichuan Basin. Therefore, the formation and maintenance of multi-layer inversions and their impacts on air quality require more exploration in the future.

4 Conclusions

Long-term and high-vertical-resolution radiosonde observations were used in this study to quantify the climatological characteristics of low-level inversions in China. Based on sounding data from 119 stations across the country during 2011–2018, this paper presented a comprehensive climatology of the spatial distributions and seasonal variations of the occurrences, depths, and strengths of inversions below 3000 m a.g.l. Both surface-based and elevated inversions are investigated. The principal results are as follows:

The east of China experiences most frequent (more than 80% of the time) low-level inversions. Inversions over the northern part are dominated by the deep strong SBIs with median thickness and strength of 200 m and 3 K, while those over the southern part by shallow weak EIs with median thickness and strength of 80 m and 0.8 K. Inversions appear fewer (around 60% of the time) over the west of China, fewest (less

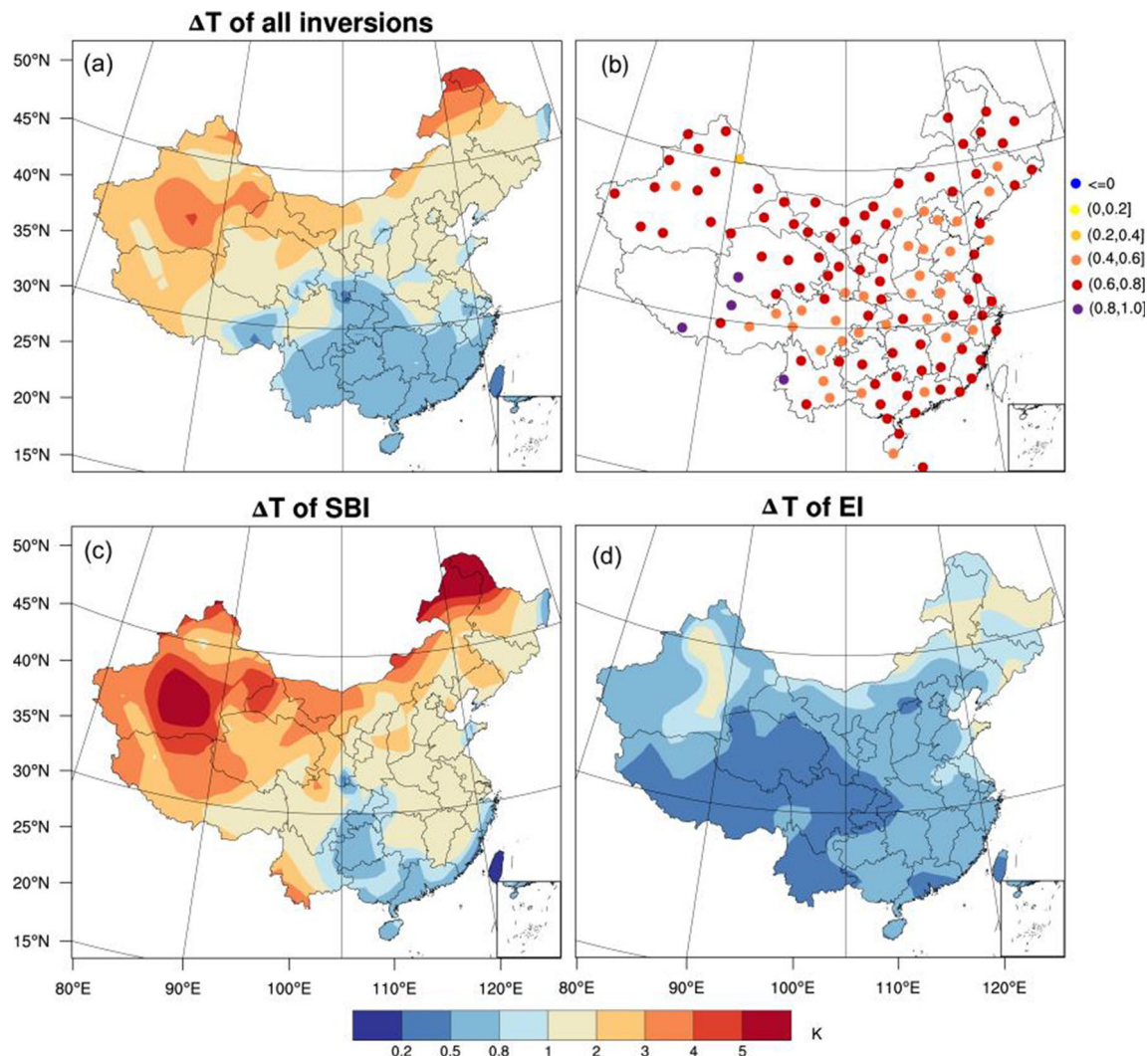


Fig. 9 Temperature differences across inversion layers (a) and its robust correlation with inversion thicknesses (b). The correlation coefficients were measured by a nonparametric method Spearman rank correlation.

The results are statistically significant at the 0.01 level based on t-test. (c) and (d) represent inversion strength for SBI and EI, respectively

than 50%) over Tibetan Plateau, and they tend to be strong thick SBIs with median depth and intensity of 170 m and 4 K. Inversion depths and strengths are positively correlated.

Notable seasonal variations are observed in occurrence frequency, depth, and intensity of inversions. They are most popular, strongest, and thickest in winter and least so in summer, with median depth ranging from 80 m in summer to 220 m in winter, and median intensity ranging from 0.3 K to 5 K, respectively. The dominant types of inversions are SBIs over the western areas all year around, whereas EIs predominate over the southeast. The northeast regions are inclined to exhibit strong deep SBIs (220 m, 5 K) in winter and weak shallow EIs (100 m, 1 K) in summer.

Four representative stations (Harbin, Urumqi, Beijing, and Chongqing) displayed the monthly variation of inversion appearances, thickness (base and top), and intensity in detail. For Harbin, strong thick SBIs (200 m, 3.8 K) are dominant in winter

while weak thin EIs (120 m, 0.8 K) in summer. By contrast, Beijing also tends to exhibit SBIs in winter and EIs in summer, but with less strength and depth (100 m, 2 K for SBIs in winter and 110 m, 0.6 K for EIs in summer). Urumqi experiences more inversions in winter than those in summer but with roughly the same probability of SBIs and EIs occurrences. The median intensity of SBIs is usually 1.2 K stronger than that of EIs. For Chongqing, seasonal variation of inversion appearances is less obvious, and shallow weak EIs (80 m, 0.4 K) predominate all year around. Sichuan Basin is characterized by multi-layer inversions below 3000 m (e.g., Zhou et al. 2015), and only the first layer is taken into consideration in this paper. Further research is required to explore the mechanisms of the cumulative effects of topography, synoptic background, moisture, aerosols, and solar radiation on behaviors of inversions.

Based on the literature review in the Introduction, low-level temperature inversions have a robust correlation with

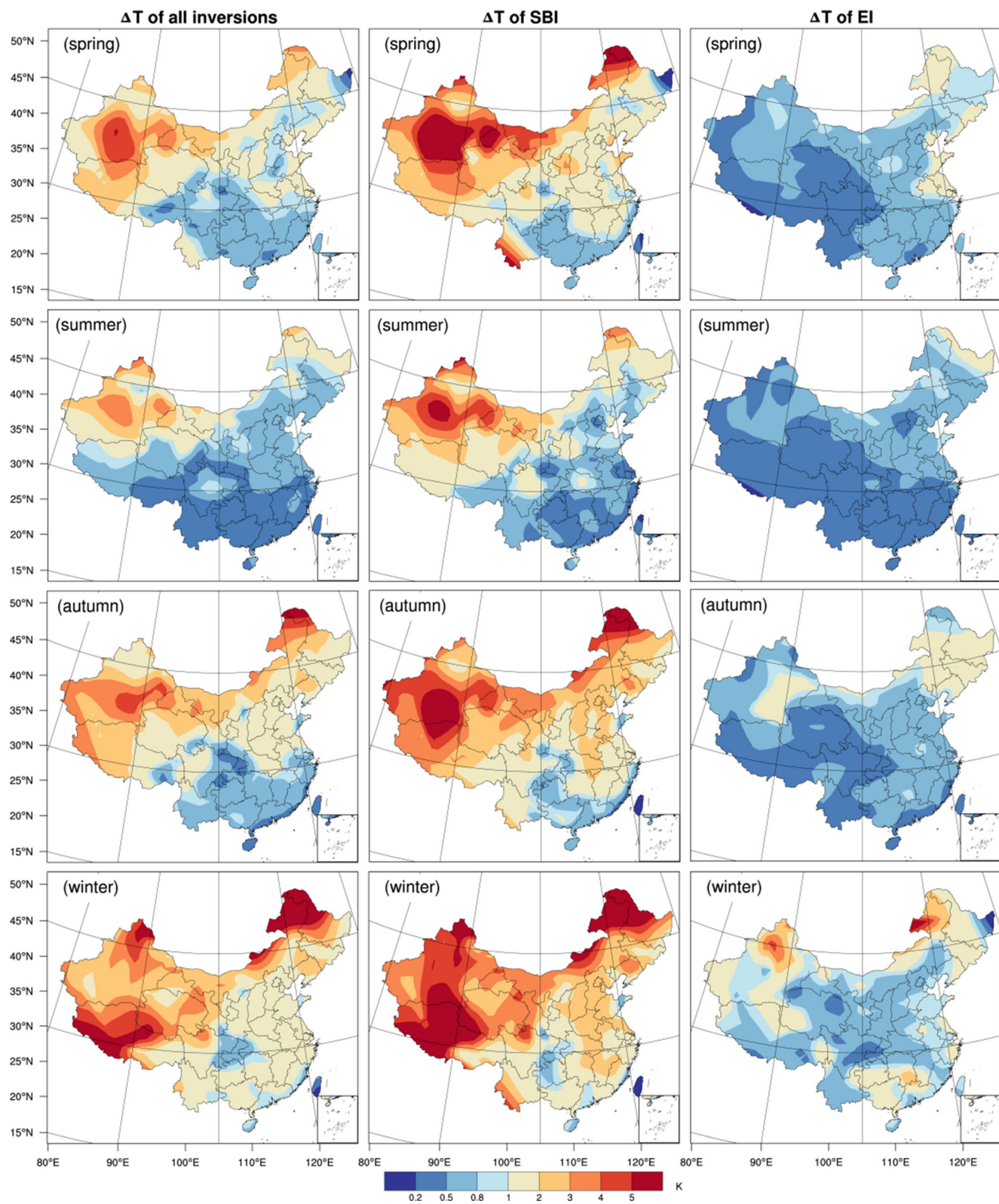


Fig. 10 Seasonal variation of the inversion strength during 2011–2018

air pollution events, since they restrict the vertical mixing of air pollutants and trap moisture in favor of the formation of secondary aerosols. The climatological characteristics

presented in this study revealed the static stability of the lower atmosphere and may make a contribution to the air pollution control.

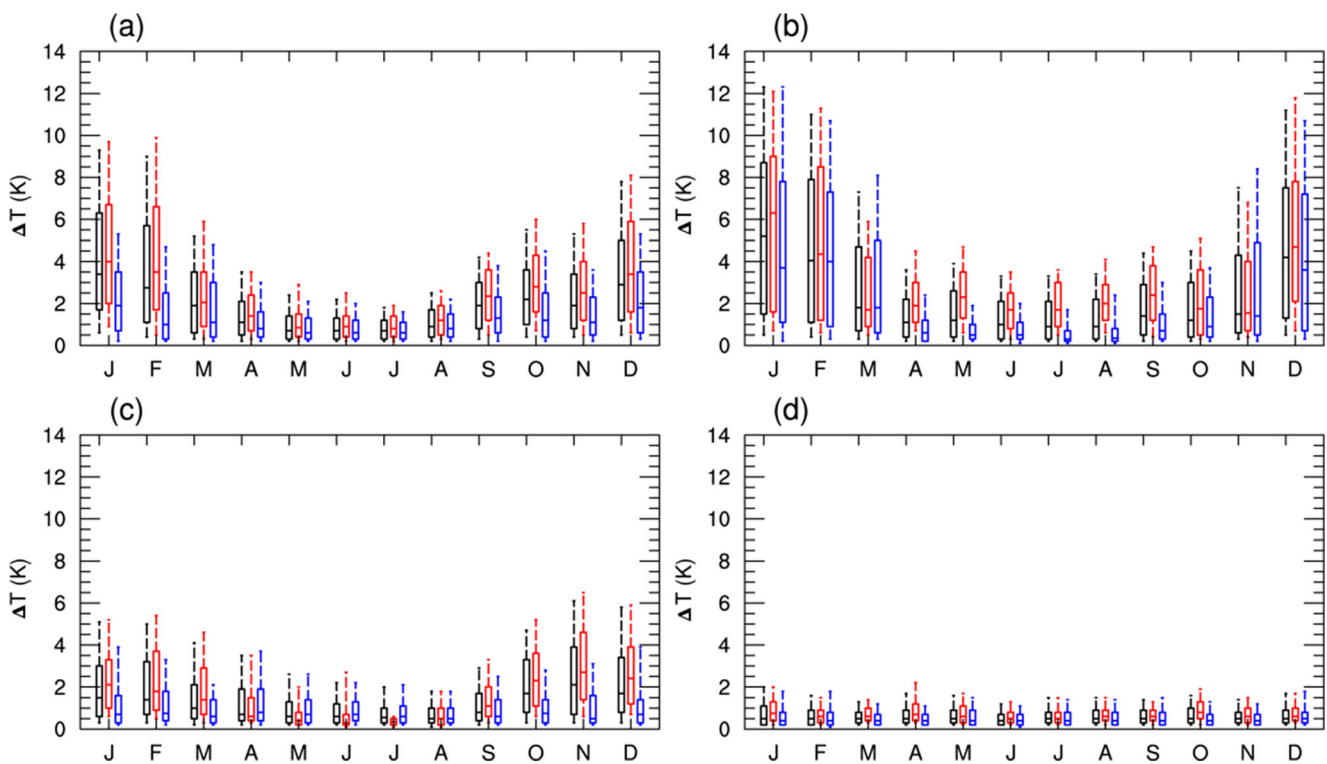


Fig. 11 Inversion strength of all inversions (black), SBI (red), and EI (blue) at four representative stations. **a**, **b**, **c**, and **d** stands for Harbin, Urumqi, Beijing, and Chongqing stations respectively. Monthly median

values are given as horizontal bars in the middle, 25 and 75% percentiles as the boxes' lower and upper boundaries, and 10 and 90% percentiles as lower and upper horizontal bars

Acknowledgements The authors are grateful to CMA for providing radiosonde data. Thanks to two anonymous referees for their insightful comments that helped improve this article.

Author contribution All authors contributed to the study conception and design. Data collection and quality control were performed by Qianhui Li. Inversion identification was performed by Qianqian Huang and Yiqi Chu. The first draft of the manuscript was written by Qianqian Huang. All authors commented on and approved the manuscript.

Funding This research was supported by Beijing Natural Science Foundation (8194060) and National Natural Science Foundation of China (41905015).

Data availability Data used in this study are available from the first author upon request (qqhuang@ium.cn).

Declarations

Competing interests/Conflict of interest The authors declare that they have no conflict of interest.

References

- Abdul-Wahab SA (2003) Analysis of thermal inversions in the Khareef Salalah region in the Sultanate of Oman. *J Geophys Res-Atmos* 109
- Abdul-Wahab SA, Al-Saifi SY, Alrumhi BA, Abdulraheem MY, Al-Uraimi M (2004) Determination of the features of the low-level temperature inversions above a suburban site in Oman using radiosonde temperature measurements: long-term analysis. *J Geophys Res-Atmos* 109(D20)
- Abdul-Wahab SA, Bakheit CS, Siddiqui RA (2005) Study the relationship between the health effects and characterization of thermal inversions in the Sultanate of Oman. *Atmos Environ* 39:5466–5471
- Bailey A, Chase TN, Cassano JJ, Noone D (2011) Changing temperature inversion characteristics in the US southwest and relationships to large-scale atmospheric circulation. *J Appl Meteorol Climatol* 50: 1307–1323
- Bourne SM, Bhatt US, Zhang J, Thoman R (2010) Surface-based temperature inversions in Alaska from a climate perspective. *Atmos Res* 95:353–366
- Brummer B, Schultze M (2015) Analysis of a 7-year low-level temperature inversion data set measured at the 280 m high Hamburg weather mast. *Meteorol Z* 24:481–494
- Cai W, Li K, Liao H, Wang H, Wu L (2017) Weather conditions conducive to Beijing severe haze more frequent under climate change. *Nat Clim Chang* 7:257–262
- Chen JL, Xiao BB, Chen CD, Wen ZF, Jiang Y, Lv MQ, Wu SJ, Li GS (2014) Estimation of monthly-mean global solar radiation using MODIS atmospheric product over China. *J Atmos Sol Terr Phys* 110:63–80
- Czarnecka M, Nidzgorska-Lencewicz J, Rawicki K (2019) Temporal structure of thermal inversions in Leba (Poland). *Theor Appl Climatol* 136:1–13
- Devasthale A, Willen U, Karlsson KG, Jones CG (2010) Quantifying the clear-sky temperature inversion frequency and strength over the Arctic Ocean during summer and winter seasons from AIRS profiles. *Atmos Chem Phys* 10:5565–5572
- Du MX, Zhang MJ, Wang SJ, Zhu XF, Che YJ (2018) Near-surface air temperature lapse rates in Xinjiang, northwestern China. *Theor Appl Climatol* 131:1221–1234

- Feng X, Wei S, Wang S (2020) Temperature inversions in the atmospheric boundary layer and lower troposphere over the Sichuan Basin. *Climatology and impacts on air pollution, China*, p 138579
- Gramsch E, Caceres D, Oyola P, Reyes E, Vasquez Y, Rubio MA, Sanchez G (2014) Influence of surface and subsidence thermal inversion on PM2.5 and black carbon concentration. *Atmos Environ* 98:290–298
- Guo LN, Huang R, Ma Y (2014) Analysis on characteristics of inversion layer and its influence on air quality in Qingdao. *Coast Eng* 33(4): 14–25
- Guo J, Miao Y, Zhang Y, Liu H, Li Z, Zhang W, He J, Lou M, Yan Y, Bian L, Zhai P (2016) The climatology of planetary boundary layer height in China derived from radiosonde and reanalysis data. *Atmos Chem Phys* 16:13309–13319
- Holmes HA, Sriramasamudram JK, Pardyjak ER, Whiteman CD (2015) Turbulent fluxes and pollutant mixing during wintertime air pollution episodes in complex terrain. *Environmental Science & Technology* 49:13206–13214
- Huang Q, Cai X, Song Y, Zhu T (2017) Air stagnation in China (1985–2014): climatological mean features and trends. *Atmos Chem and Phys* 17:7793–7805
- Huang Q, Cai X, Wang J, Song Y, Zhu T (2018) Climatological study of the Boundary-layer air Stagnation Index for China and its relationship with air pollution. *Atmos. Chem. and Phys.* 18:7573–7593
- Jakobson L, Vihma T, Jakobson E, Palo T, Mannik A, Jaagus J (2013) Low-level jet characteristics over the Arctic Ocean in spring and summer. *Atmos Chem Phys* 13:11089–11099
- Ji F, Evans JP, Di Luca A, Jiang N, Olson R, Fita L, Arüeso D, Chang LTC, Scorgie Y, Riley M (2018) Projected change in characteristics of near surface temperature inversions for southeast Australia. *Clim Dyn* 52:1487–1503
- Kahl JD (1990) Characteristics of the low-level temperature inversions along the Alaska Arctic coast. *Int J Climatol* 10:537–548
- Kahl JDW, Martinez DA, Zaitseva NA (1996) Long-term variability in the low-level inversion layer over the Arctic Ocean. *Int J Climatol* 16:1297–1313
- Kassomenos PA, Paschalidou AK, Lykoudis S, Koletsis I (2014) Temperature inversion characteristics in relation to synoptic circulation above Athens, Greece. *Environ Monit Assess* 186:3495–3502
- Katsoulis BD (1988) Aspects of the occurrence of persistent surface inversions over Athens Basin, Greece. *Theor Appl Climatol* 39:98–107
- Largeron Y, Staquet C (2016) Persistent inversion dynamics and wintertime PM10 air pollution in Alpine valleys. *Atmos Environ* 135:92–108
- Leukauf D, Gohm A, Rotach MW, Wagner JS (2015) The impact of the temperature inversion breakup on the exchange of heat and mass in an idealized valley: sensitivity to the radiative forcing. *J Appl Meteorol Climatol* 54:2199–2216
- Li J, Chen HB, Li ZQ, Wang PC, Cribb M, Fan XH (2015a) Low-level temperature inversions and their effect on aerosol condensation nuclei concentrations under different large-scale synoptic circulations. *Adv Atmos Sci* 32:898–908
- Li X, Xia X, Wang L, Cai R, Zhao L, Feng Z, Ren Q, Zhao K (2015b) The role of foehn in the formation of heavy air pollution events in Urumqi, China. *J Geophys Res-Atmos* 120:5371–5384
- Liao T, Gui K, Jiang W, Wang S, Wang B, Zeng Z, Che H, Wang Y, Sun Y (2018) Air stagnation and its impact on air quality during winter in Sichuan and Chongqing, southwestern China. *Sci Total Environ* 635:576–585
- Liu YH, Key JR, Schweiger A, Francis J (2006) Characteristics of satellite-derived clear-sky atmospheric temperature inversion strength in the Arctic, 1980–96. *J Clim* 19:4902–4913
- Liu L, Li ZQ, Yang X, Gong HN, Li C, Xiong AY (2016) The long-term trend in the diurnal temperature range over Asia and its natural and anthropogenic causes. *J Geophys Res-Atmos* 121:3519–3533
- Mahesh A, Walden VP, Warren SG (1997) Radiosonde temperature measurements in strong inversions: correction for thermal lag based on an experiment at the South Pole. *J Atmos Ocean Technol* 14:45–53
- Milionis AE, Davies TD (2008) A comparison of temperature inversion statistics at a coastal and a non-coastal location influenced by the same synoptic regime. *Theor Appl Climatol* 94:225–239
- Munoz RC, Zamora RA, Ruttlant JA (2011) The coastal boundary layer at the eastern margin of the Southeast Pacific (23.4 degrees S, 70.4 degrees W): cloudiness-conditioned climatology. *J Clim* 24:1013–1033
- Nidzgorska-Lencewicz J, Czarnecka M (2015) Winter weather conditions vs. air quality in Tricity, Poland. *Theor Appl Climatol* 119: 611–627
- Nodzu MI, Ogino SY, Tachibana Y, Yamanaka MD (2006) Climatological description of seasonal variations in lower-tropospheric temperature inversion layers over the Indochina Peninsula. *J Clim* 19:3307–3319
- Palarz A, Celinski-Myslaw D, Ustrnul Z (2019) Temporal and spatial variability of elevated inversions over Europe based on ERA-interim reanalysis. *Int J Climatol* 40:1335–1347
- Pietroni I, Argentini S, Petenko I (2014) One year of surface-based temperature inversions at Dome C, Antarctica. *Bound-Layer Meteorol* 150:131–151
- Prezerakos NG (1997) Lower tropospheric structure and synoptic scale circulation patterns during prolonged temperature inversions over Athens, Greece. *Theor Appl Climatol* 60:63–76
- Schiemann R, Luethi D, Schaer C (2009) Seasonality and interannual variability of the westerly jet in the Tibetan Plateau region. *J Clim* 22:2940–2957
- Seidel DJ, Ao CO, Li K (2010) Estimating climatological planetary boundary layer heights from radiosonde observations: comparison of methods and uncertainty analysis. *J Geophys Res-Atmos* 115
- Seidel DJ, Zhang Y, Beljaars A, Golaz JC, Jacobson AR, Medeiros B (2012) Climatology of the planetary boundary layer over the continental United States and Europe. *J. Geophys. Res.-Atmos.* 117
- Shi Y (2016) An analysis of the diurnal temperature range in China and its association with the diurnal variation of precipitation. Nanjing University of Information Science and Technology
- Shi C, Nduka IC, Yang Y, Huang Y, Yao R, Zhang H, He B, Xie C, Wang Z, Yim SHL (2020) Characteristics and meteorological mechanisms of transboundary air pollution in a persistent heavy PM2.5 pollution episode in Central-East China. *Atmospheric Environment* 223
- Stryhal J, Huth R, Sladek I (2017) Climatology of low-level temperature inversions at the Prague-Libu aerological station. *Theor Appl Climatol* 127:409–420
- Thomas MA, Devasthale A, Tjernstrom M, Ekman AML (2019) The relation between aerosol vertical distribution and temperature inversions in the Arctic in winter and spring. *Geophys Res Lett* 46:2836–2845
- Tjernstrom M, Graversen RG (2009) The vertical structure of the lower Arctic troposphere analysed from observations and the ERA-40 reanalysis. *Q J R Meteorol Soc* 135:431–443
- Vihma T, Kilpelainen T, Manninen M, Sjöblom A, Jakobson E, Palo T, Jaagus J, Maturilli M (2011) Characteristics of temperature and humidity inversions and low-level jets over Svalbard fjords in spring. *Adv Meteorol* 2011:1–14. <https://doi.org/10.1155/2011/486807>
- Wang SYS, Hippis LE, Chung OY, Gillies RR, Martin R (2015) Long-term winter inversion properties in a mountain valley of the western United States and implications on air quality. *J Appl Meteorol Climatol* 54:2339–2352
- Wetzel C, Brummer B (2011) An Arctic inversion climatology based on the European Centre Reanalysis ERA-40. *Meteorol Z* 20:589–600
- Wu Y, Ge X, Wang J, Shen Y, Ye Z, Ge S, Wu Y, Yu H, Chen M (2018) Responses of secondary aerosols to relative humidity and

- photochemical activities in an industrialized environment during late winter. *Atmos Environ* 193:66–78
- Xia M, Zhou W, Pei H, Dai Z (2017) Characteristic analysis of lower-level temperature inversion over Nanjing based on L-band radar data. *Trans Atmos Sci* 40:562–569
- Xu YZ, Yang WD, Wang JZ (2017) Air quality early-warning system for cities in China. *Atmos Environ* 148:239–257
- Xu T, Song Y, Liu M, Cai X, Zhang H, Guo J, Zhu T (2019) Temperature inversions in severe polluted days derived from radiosonde data in North China from 2011 to 2016. *Sci Total Environ* 647:1011–1020
- Zhang YH, Seidel DJ, Golaz JC, Deser C, Tomas RA (2011a) Climatological characteristics of Arctic and Antarctic surface-based inversions. *J Clim* 24:5167–5186
- Zhang YH, Zhang SD, Yi F, Chen ZY (2011b) Statistics of lower tropospheric inversions over the continental United States. *Ann Geophys* 29:401–410
- Zhong J, Zhang X, Wang Y, Sun J, Zhang Y, Wang J, Tan K, Shen X, Che H, Zhang L, Zhang Z, Qi X, Zhao H, Ren S, Li Y (2017) Relative contributions of boundary-layer meteorological factors to the explosive growth of PM_{2.5} during the red-alert heavy pollution episodes in Beijing in December 2016. *Journal of Meteorological Research* 31:809–819
- Zhong W, Yin Z, Wang H (2019) The relationship between anticyclonic anomalies in northeastern Asia and severe haze in the Beijing-Tianjin-Hebei region. *Atmos Chem Phys* 19:5941–5957
- Zhou G (2010) Studies of the influence of meteorological factors on air pollution and its numerical simulation in the main urban region of Chongqing. Lanzhou University
- Zhou S, Ni C, Liu P (2015) Characteristics of temperature inversion in atmospheric boundary layer in Chengdu area. *Journal of Meteorology and Environment* 31:108–111
- Zhu X, He H, Liu M, Yu G, Sun X, Gao Y (2010) Spatio-temporal variation of photosynthetically active radiation in China in recent 50 years. *J Geogr Sci* 20:803–817
- Zhu WH, Xu XD, Zheng J, Yan P, Wang YJ, Cai WY (2018) The characteristics of abnormal wintertime pollution events in the Jing-Jin-Ji region and its relationships with meteorological factors. *Sci Total Environ* 626:887–898

Publisher's note Springer Nature remains neutral with regard to jurisdictional claims in published maps and institutional affiliations.